MICROBOONE-NOTE-1018-PUB

Study of Space Charge Effects in MicroBooNE

The MicroBooNE Collaboration

November 29, 2016

We present a study of the impact of space charge effects within the MicroBooNE liquid argon time projection chamber (LArTPC). The space charge effect is the build-up of slow-moving positive ions in a detector due to, for instance, ionization from cosmic rays, leading to a distortion of the electric field within the detector. This effect leads to a displacement in the reconstructed position of signal ionization electrons in LArTPC detectors, as well as variations in the amount of charge quenching experienced by ionization throughout the volume of the TPC. The LArTPC utilized in MicroBooNE is expected to be modestly impacted from the space charge effect, with the electric field magnitude changing by up to 15% (at a drift field of 273 V/cm) in some locations within the TPC. Studying tracks in the TPC matched to an external small cosmic ray counter system, we observe offsets in the reconstructed track ends from their expected positions at the TPC edges, consistent with the presence of space charge effects in the detector. Data is compared to a simulation including space charge effects, which reproduces the observed track distortions. Finally, the derivation of a correction for the reconstruction of track direction is described, illustrating how one might remove the impact of these effects within the MicroBooNE LArTPC.

1 Introduction

In order to correctly reconstruct the trajectories of particles that travel through the MicroBooNE liquid argon time projection chamber (LArTPC), it is essential to know very well the magnitude and direction of the drift electric field throughout the active volume of the TPC. Nominally the electric field should be uniform throughout the TPC volume. However, field effects such as the space charge effect may cause distortions in the electric field that result in distortions in the reconstructed position of ionization electron clusters detected by the TPC wire planes. We have performed a study of such effects by looking at tracks reconstructed in the TPC and matched to small external

muon counters. Fig. 1 shows the start/end points of reconstructed tracks for minimum ionizing particles (MIPs) for off-beam data in the MicroBooNE TPC projected onto the x–y plane (where x is the ionization drift direction, y is the direction along the zenith axis, and z is the beam direction). Instead of being distributed uniformly along the borders, the points exhibit an offset from the edges of the TPC that increases in magnitude with the x coordinate (in the direction of the cathode).

The observation illustrated in Fig. 1 is consistent with what one would expect from the presence of space charge effects in the active volume of the TPC. The effect on the operation of a vacuum diode of a spatially varying distribution of free electrons, commonly called space charge, was first considered by Child [1] and Langmuir [2]. In that example, electrons are released from a hot cathode at low velocity and drift freely under the influence of the local electric field as modified by the drifting electrons. The space charge effect in LArTPC detectors results from the build-up of slow-moving positive ions in a detector due to, for instance, ionization from cosmic muons. As MicroBooNE is an experiment on the surface with little overburden, the cosmic muon flux (20–30 muons per 4.8 ms readout window at a drift field of 273 V/cm) is expected to create a significant amount of charge build-up from positive argon ions that could modestly impact the drift electric field within the TPC active volume. Resultant distortions in the drift electric field would lead to different amounts of charge quenching (recombination) in different parts of the TPC and would also lead to spatial distortions in the trajectories of reconstructed particle tracks and electromagnetic showers. Because the positive ions tend to draw drifting ionization electrons closer to the center of the TPC, tracks reconstructed closer to the cathode would have start/end points that are offset from the edges of the TPC active volume, as is observed in Fig. 1.

Given the observation discussed above and the possible implication of the space charge effect, we present a study comparing spatial distortions from the space charge effect (SCE) predicted in simulation with those observed in data. The focus of this note is the SCE in the directions transverse to ionization drift at the y and z boundaries of the TPC where the effect is strongest. The SCE in the ionization drift direction (x) is not covered in the analysis presented in this note, and remains the subject of a future analysis. Furthermore, a complete calibration of the space charge effect throughout the entire active TPC volume is not attempted at present and is similarly planned for future study [3], which will include the use of a UV laser system installed at MicroBooNE [4]. Instead, the goal in this note is to show that a data-derived correction of the SCE can improve tracking performance on a very specific track sample: cosmic muon tracks tagged by the Muon Counter System (MuCS), which we describe in Sec. 4.

This note is structured as follows: first we provide a thorough set of definitions used to reference specific distortions of reconstructed ionization electron cluster position due to the space charge effect, differentiating between various directions and boundaries of the active TPC volume. Next we briefly discuss the simulation of SCE used to compare against observations of the effect in data. Following this section is a description of the MuCS, which is used to tag tracks at precise locations in the drift direction with respect to the anode plane, a useful sample for studying the SCE. Next the measurement of distortions in reconstructed ionization electron cluster position due to the space charge

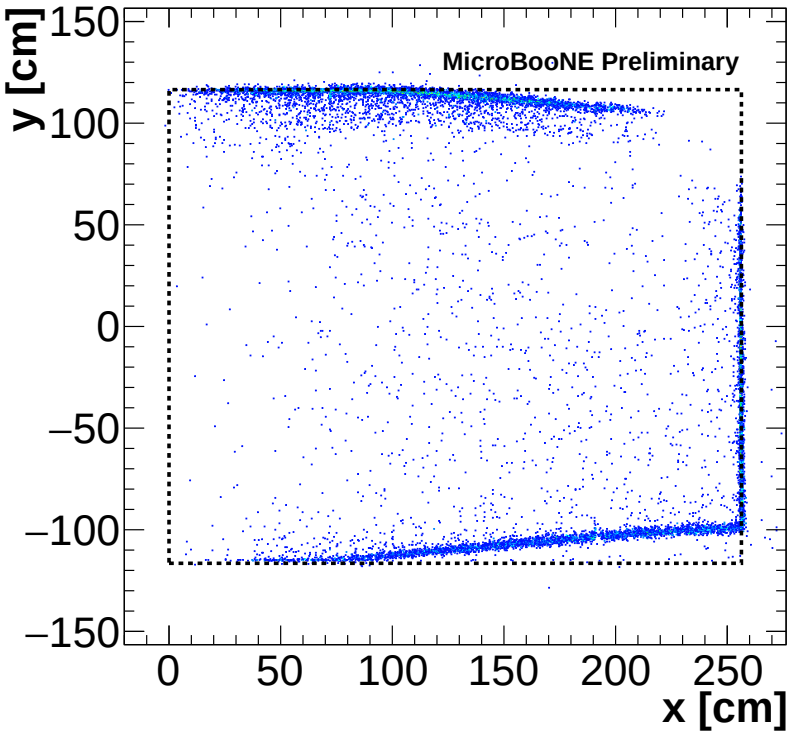

Figure 1: Start/end points of reconstructed cosmic muon tracks tagged by an external muon counter in the x–y plane for off-beam (cosmic) events. In absence of detector effects, the points should be distributed along the borders (dashed lines). Note that the anode is located at $x = 0$ cm while the cathode is at $x = 256$ cm.

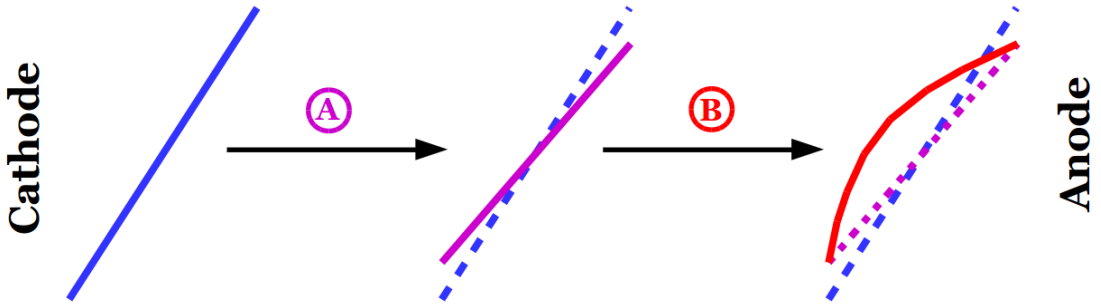

Figure 2: Impact of the space charge effect on reconstructed tracks in the detector. The impact on a reconstructed track can be broken up into two distinct features: a squeezing of the sides of the tracks in the transverse TPC directions that can somewhat resemble a rotation ("A") and a bowing of the track toward the cathode that is most pronounced in the middle of the TPC ("B").

effect is described in detail, for various directions and locations in the MicroBooNE TPC. The derivation of a correction that improves the reconstruction of track direction is then described, including the utilization of MuCS-tagged tracks to validate that the correction improves tracking performance by making use of measured positions of the MuCS boxes. Finally, we discuss conclusions from this initial study of the SCE at MicroBooNE, including future plans for calibrating out the effect more fully within the TPC.

2 Definitions

Within the context of this note, when we discuss the space charge effect, we specifically refer to distortions in the reconstructed ionization electron cluster position, not the underlying distortions of the electric field that yield these spatial offsets. However, the distortion of the electric field throughout the volume of the TPC will lead to spatial variations in the amount of recombination that is experienced by ionizing particles, as well as variations in scintillation light yield produced during particle interactions in the liquid argon, and is an important topic for future study.

SCE defined in this way (as spatial distortions) can be decomposed from a vector quantity into three offsets in reconstructed ionization electron cluster position:

$$\Delta x = x_{\text{reco}} - x_{\text{true}}, \tag{1}$$

$$\Delta y = y_{\text{reco}} - y_{\text{true}}, \tag{2}$$

and

$$\Delta z = z_{\text{reco}} - z_{\text{true}}, \tag{3}$$

where x_{reco}, y_{reco}, and z_{reco} represent the reconstructed ionization electron cluster position coordinates and x_{true}, y_{true}, and z_{true} represent the true position coordinates of

ionization deposition in the active TPC volume. Note that when we refer to the simulated effects of space charge in reconstructing ionization electron cluster positions, we use the "reco" and "sim" qualifiers interchangeably (as we do not simulate other sources of distortions). In general, these spatial distortions are also dependent on the three-dimensional position in the TPC:

$$\Delta x = \Delta x(x_{\text{true}}, y_{\text{true}}, z_{\text{true}}), \tag{4}$$

$$\Delta y = \Delta y(x_{\text{true}}, y_{\text{true}}, z_{\text{true}}), \tag{5}$$

$$\Delta z = \Delta z(x_{\text{true}}, y_{\text{true}}, z_{\text{true}}). \tag{6}$$

When we refer to these quantities, we will generally drop the "true" qualifier, e.g. $\Delta y(x, y, z)$.

Often we will want to refer to dependencies of the spatial distortions in only one particular direction (or maybe two). This is because either (a) there is expected to be negligible variation in the magnitude of the distortion with respect to the other direction(s) in the region of the TPC considered, (b) the region of the TPC spanned by the track sample being used is of limited extent in one or more directions (as is the case for MuCS-tagged tracks with respect to z direction), or (c) the value of one or more coordinates is fixed, as is the case when looking at distortions at one of the TPC boundaries. Under one of these circumstances we simply omit the other coordinates in the variable, e.g. $\Delta y(x)$. In case (c) we will often differentiate between the different TPC boundaries by adding a subscript to the distortion variable, e.g. $\Delta y_{\text{top}}(x)$ when discussing measurements of $\Delta y(x)$ at the top of the TPC. In other cases we may discuss spatial distortions generically without referencing particular locations in the TPC; in this case we simply drop all coordinates, e.g. Δy.

When discussing the measurements in Sec. 6.1 and Sec. 6.2, we will refer to $\Delta y(x)$, $\Delta y(z)$, and $\Delta z(y)$, where the independent variables are reconstructed quantities (not the true positions of ionization deposition in the TPC). In the regions of the TPC where the measurements are carried out, the differences between the true coordinates and the reconstructed coordinates are very small for the independent variables of interest. In parts of the note where the true and reconstructed quantities could be easily conflated, more explicit notation is used.

3 Simulation

Software was developed to simulate the impact of space charge on the electric field within the TPC, along with the distortions in reconstructed ionization electron position at different points within the TPC volume. This simulation makes use of a Fourier series solution to the boundary value problem to solve for the electric field on a three-dimensional grid within the volume of the TPC, an interpolation in between the grid points using radial basis functions to find the electric field everywhere in the TPC, and ray-tracing

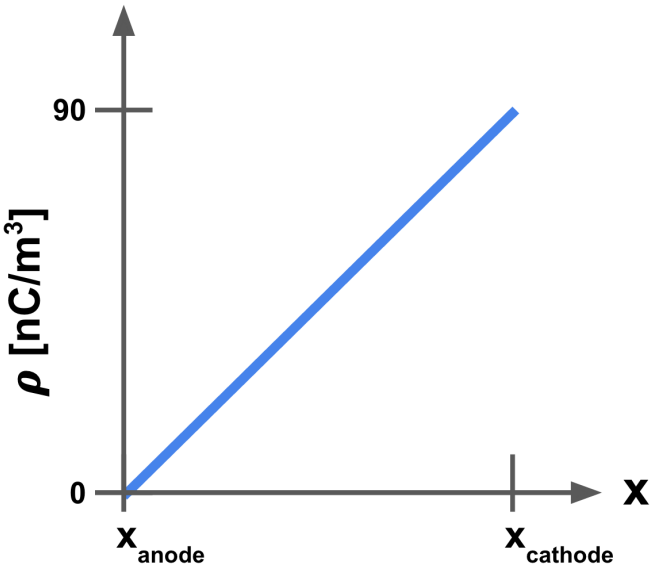

Figure 3: Space charge density ρ as a function of the x position assumed in the simulation. The space charge density at the cathode, 90 nC/m^3, reflects both the expected rate of cosmic ray charge deposition and effects of recombination [5]. The distribution is independent of y and z in the simulation (an approximation).

using the RKF45[1] method in order to simulate the distortions in reconstructed position of ionization electron clusters.

An assumption is made that the charge deposition rate from cosmic muons is uniform across the TPC volume: $2{\times}10^{-10}$ C/m^3/s at a drift field of 500 V/cm [5], with a recombination correction for a drift field of 273 V/cm yielding a value ∼25% smaller for the present study. As a result, ignoring higher-order effects of the electric field distortions on the space charge configuration itself, the space charge density is linear with respect to the distance from the anode plane. The space charge density profile used in the simulation is shown in Fig. 3 for a drift field of 273 V/cm.

Some of the simulation results are shown in Fig. 4 and Fig. 5, which illustrate the impact of space charge on both the drift electric field (Fig. 4) as well as the distortions in reconstructed ionization electron cluster position (Fig. 5). At a drift field of 273 V/cm (corresponding to early data-taking at MicroBooNE), the expected maximal impact on the electric field is roughly 10% in both the drift and transverse directions.

While the simulation provides a useful order-of-magnitude estimation of the distortions in reconstructed ionization electron cluster position within the MicroBooNE TPC, and provides basic shape features that we might expect in the data, there are several understood limitations of the simulation. First of all, the flow of liquid argon, which may

[1] "Runge–Kutta–Fehlberg 4(5)" method, an algorithm for the numerical solution of ordinary differential equations.

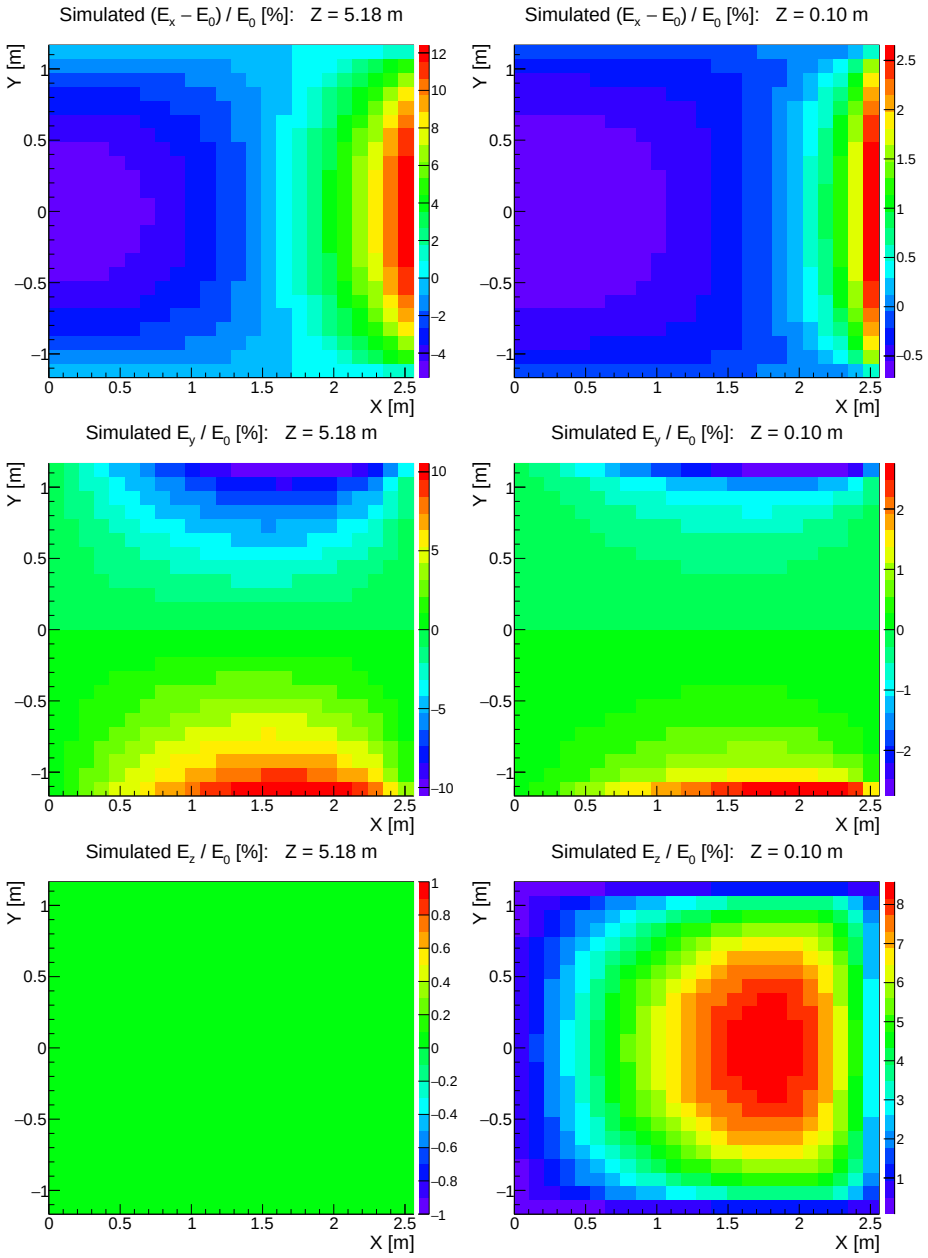

Figure 4: Illustration of the simulated effects of space charge on the drift electric field in the MicroBooNE TPC, as described in Sec. 3. Results are shown for the effect in x (top row), y (middle row), and z (bottom row). The electric field distortions are normalized to the nominal drift electric field magnitude (E_0) of 273 V/cm and are plotted as a function of the true position in the TPC. Simulation results are shown both for a central slice in z (left column) and for a slice in z closer to the end of the TPC, $z = 10$ cm (right column).

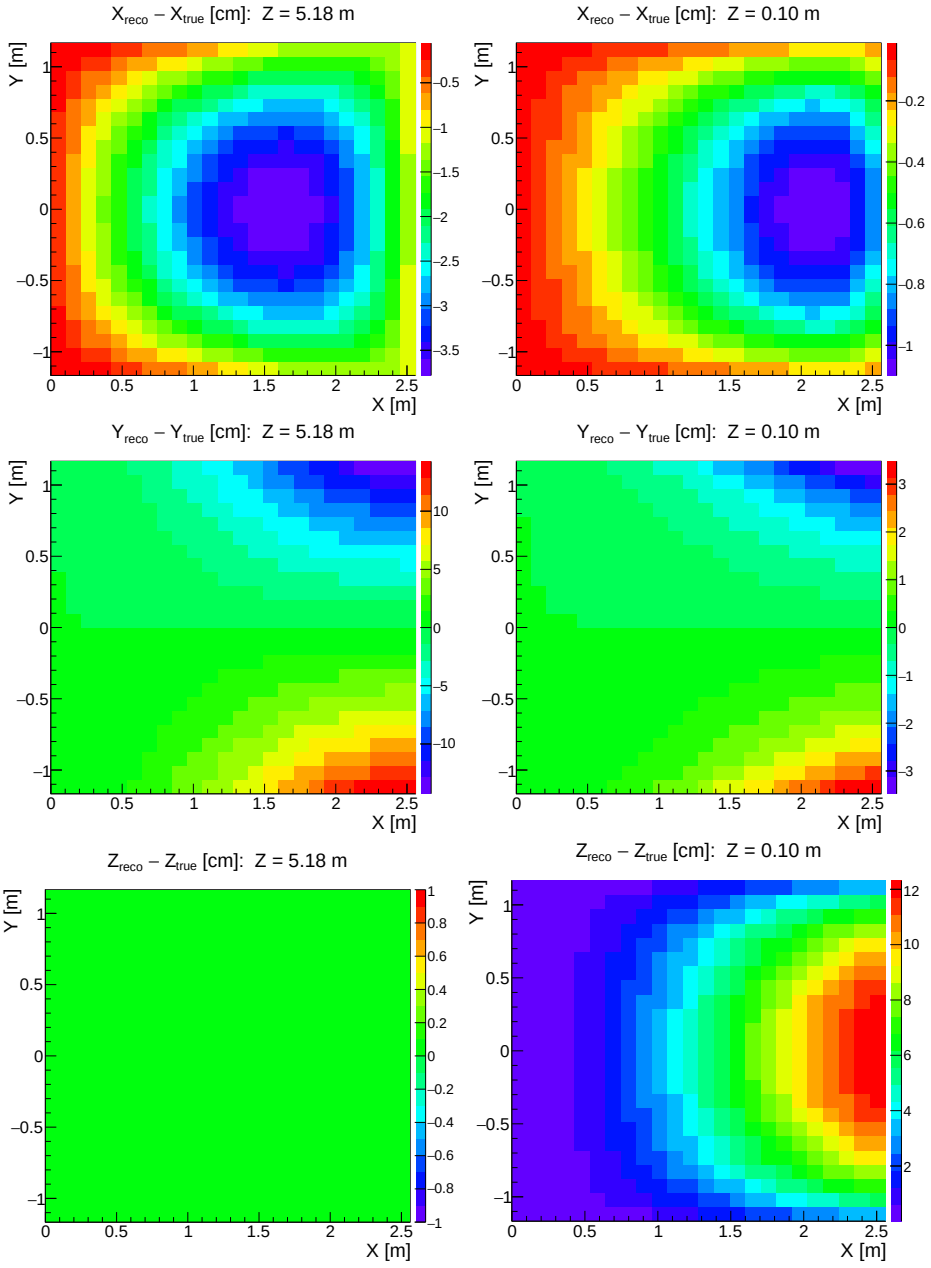

Figure 5: Illustration of the simulated effects of space charge on the distortions in reconstructed ionization electron cluster position in the MicroBooNE TPC, as described in Sec. 3. Results are shown for the effect in x (top row), y (middle row), and z (bottom row). The distortions in reconstructed ionization electron cluster position are shown in units of cm and are plotted as a function of the true position in the TPC. Simulation results are shown both for a central slice in z (left column) and for a slice in z closer to the end of the TPC, $z = 10$ cm (right column).

move positive argon ions in or out of the active TPC volume, is not considered. Also, the assumption of uniform charge deposition from cosmic rays throughout the TPC may not be the case in reality as enhanced cosmogenic activity near the top of the detector may lead to greater ion production rates closer to the top of the TPC active volume. Finally, the linear space charge density assumed in the simulation (see Fig. 3) approximates the ion drift speed (roughly 5 mm/s at a drift field of 273 V/cm) as constant throughout the TPC, while in reality the electric field distortions arising from the SCE itself would break this assumption.

4 MuCS Description

The MuCS consists of two sets of "X-Y" modules made up of scintillator strips placed into two separate, light-tight boxes and readout via wavelength shifting fibers connected to Multi-Anode PMTs. Each X-Y module is made up two sets of 24 scintillator strips arranged into bi-layers oriented perpendicular to each other [6]. The PMTs are readout by a DAQ system that is separate from the DAQ system that reads out the TPC and PMT systems.

The MuCS is a small system designed to form a trigger on through-going muons that intersect two planes of scintillator strips that can be configured in various spatial configurations. The trigger from the MuCS is propagated to the MicroBooNE trigger system to trigger a full TPC and PMT readout. With the MuCS trigger in place, the t_0 for a track associated with the MuCS is known and so these tracks are useful for various detector physics and reconstruction studies.

For this note, all MuCS data and MC samples have the MuCS in the same configuration depicted in Fig. 6. In this configuration, greater than 99% of muon trajectories that trigger the MuCS system are expected to intersect the TPC active volume. These trajectories are directed away form the anode.

There are two data-taking configurations available with the MuCS DAQ system. In the first mode, trigger-only mode, only a trigger is sent for TPC readout and no information about the hit-patterns seen by the MuCS is saved. This is the normal mode of operation for the MuCS and the triggers from this mode are collected as part of the MuCS production data stream that has been running constantly since December 2015. In this mode the scintillator strips act only effectively as unified paddles with no granular information coming from the scintillator strips.

In the second mode, trigger-readout mode, a trigger is sent to the TPC readout as in the first mode, but the MuCS DAQ is also running and saving the hit patterns seen in the scintillator strips of the PMTs. The data then follows a processing path that merges the MuCS hit patterns and reconstructed trajectory information with the TPC and PMT data stream.

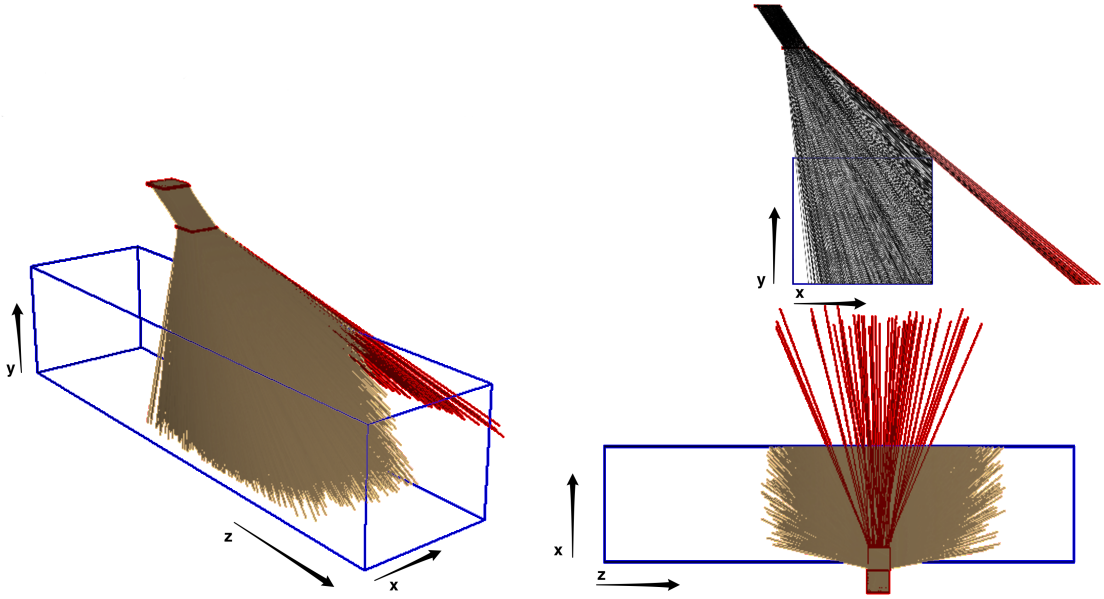

Figure 6: MuCS trajectories possible in the current configuration of the boxes. The brown tracks are those that intersect the TPC while the red tracks miss the TPC.

5 Dataset and Reconstruction

The datasets used in this note are either triggered by the MuCS or are Booster-Neutrino Beam (BNB) triggered data and are referred to as MuCS or BNB samples, respectively. The MuCS and BNB samples have both data and MC counterparts. Furthermore, the MuCS samples are divided into MuCS-tagged (using the MuCS trigger-only mode) and MuCS-merged (using the MuCS-trigger-readout mode) samples, as described in Sec. 4.

All data and MC uses the same reconstruction methods based in the LArSoft software framework [7].

5.1 MuCS Samples

The MuCS-tagged MC samples use the CRY cosmic ray generator [8] to generate one muon per event at the position of the top box of the MuCS and it is checked for intersection with both boxes. If it does not intersect both boxes, it is discarded and another muon generated until an intersection with both boxes is found.

The MuCS-tagged data samples used in this note are from the MuCS production data stream. The MuCS triggers at a rate of nearly 3 Hz and this rate is prescaled by 100 before sending the signal to trigger readout. In the general data stream then, a MuCS trigger is issued at a rate of 0.02 Hz or roughly one per minute. The samples used in this note consist of data acquired from March 1, 2016 to March 9, 2016 and contain 7,257 events.

The MuCS-merged sample used in this note was taken in November of 2015 and contains 17,350 TPC events. There are 11,213 events (65%) in this sample that have been successfully merged via the process described in Sec. 4. To produce a matched MC sample, a 4 GeV Monte Carlo muon with the same starting point and trajectory as the measured in data by the MuCS is generated. This produces a reconstructed MIP MC track that can then be compared with the reconstructed data track.

From the reconstruction stage onward each sample follows the same path. In this note, a Kalman Hit Filter [9] reconstruction algorithm is used for tracks.

After the reconstruction stage has produced the track data product the process of tagging the tracks, or producing an association between a track and cosmic tag data product, is carried out next and in the same manner for every sample. The reconstructed track is propagated back to the y (vertical) position of each MuCS box using the starting direction of the track [6]. If this new position is within the x and z boundaries of the MuCS box then the track is tagged with a cosmic tag that uniquely identifies it as MuCS-tagged. This tagging process is identical for data and MC.

5.2 BNB and Cosmic Samples

To compare SCE at the edges of the TPC boundaries a data sample of cosmic rays is used in both data and MC. The data sample used is a BNB-triggered dataset consisting of 10,917 events. The cosmic rays, primarily muons, contained in the BNB trigger readout window enable the analysis of measured track start/end points at the physical boundaries of the TPC active volume.

6 Results

6.1 SCE Data/MC Comparison with MuCS-tagged Tracks

MuCS-tagged tracks can be utilized to determine SCE offsets near the boundaries of the TPC. The advantage of using tracks tagged in this way is the ability to pin down the position of the track in the drift direction, x, by firing the TPC trigger when a track passes through the MuCS, which provides the time of the initial track energy deposition in the TPC, t_0. This allows us to determinate the SCE offsets as a function of the distance from the anode planes. In principle this information is also obtainable from the light-collection system at MicroBooNE, which can also yield information about t_0. However, the tag from the MuCS is much less ambiguous and provides a nearly pure sample of tracks with correctly determined position in the drift direction. The one disadvantage to utilizing the MuCS in this measurement is limited coverage of the TPC in the z direction.

With the MuCS position used for the study presented here, the determination of the SCE offsets in the y direction as a function of the drift direction, $\Delta y(x)$, is possible at the top and bottom of the TPC in y and near center of the TPC in the z direction. This is a particularly interesting region of the detector to characterize SCE distortions as the effect is expected to be strongest in this part of the detector. While distortions due to

SCE in the y direction can be quite large here, distortions in the x and z directions are expected to be very small, allowing us to cleanly isolate one component of the effect.

In order to determine $\Delta y(x)$ at the boundaries of the TPC in y, we utilize the fact that the start/end points of reconstructed through-going (passing completely through the entire active TPC volume) tracks from cosmic muons would be physically separated from the TPC edges in parts of the detector where SCE distortions are significant. For muons passing through the MuCS, this would result in tracks appearing to begin below the top of the TPC and terminate before the bottom of the TPC. After reconstructing the tracks tagged by the MuCS, we group the track start/end points into bins in x, separately for the top of the TPC and bottom of the TPC. For each bin in x, we obtain a histogram of track start/end points in terms of their location in y. A Gaussian fit to the core of the y distribution near the mode is used to extract Δy for the particular bin in x. The uncertainty on the Gaussian mean from the fit represents the uncertainty in the position of the mode of the distribution, which we identify as the uncertainty in the measurement of Δy in the given bin.

The results of the measurement of $\Delta y(x)$ are shown in Fig. 7 and Fig. 8. Both distributions from simulation and the measurement using actual data are shown, with separate results for the top of the TPC and bottom of the TPC. A couple of observations can be made with this result in hand. First of all, the magnitude of the distortions in data are very similar to those predicted by simulation, with similar features observed in the shape of the distribution when comparing data and simulation. Additionally, it appears that there is a negligible level of SCE within 60–90 cm from the anode at both the top of the TPC and bottom of the TPC when looking at data. This may be indicative of liquid argon flow washing out the space charge distribution near the TPC anode. A comparison between data and MC can be made more easily by eye in Fig. 9, where both data and MC are shown.

It is possible to study the stability of the space charge configuration over time by repeating the measurement outlined above for different data-taking runs. Comparing a dataset collected in November 2015 with one taken in March 2016 (Fig. 10), we see very little change in spatial distortions of tracks at the top and bottom of the TPC: the largest difference observed is $\sim$1 cm. While this seems to suggest that a space charge calibration may not need to be done very frequently, we should note that it is important to probe finer timescales than the one accessed with the comparison shown in Fig. 10. We intend to study these timescales in the future.

It is possible to extend this study to the measurement of $\Delta z(x)$ near the ends of the TPC in z. This would require moving the MuCS to a different position and angle on the detector platform such that cosmic muons pass through the MuCS and then through an end of the TPC in z. Additionally, a more complete measurement can be made throughout the majority of the active TPC volume by utilizing a larger cosmic ray tagger system and/or a UV laser calibration system. These studies are planned for the future as well.

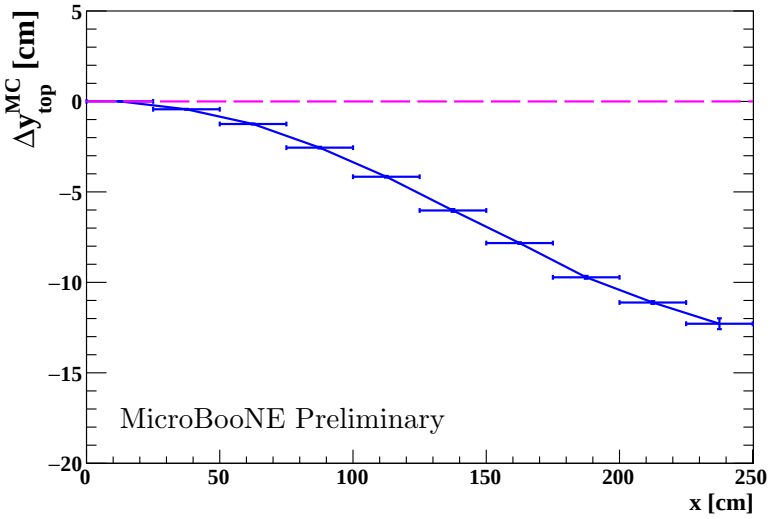

(a) $\Delta y^{\mathrm{MC}}_{\mathrm{top}}(x)$

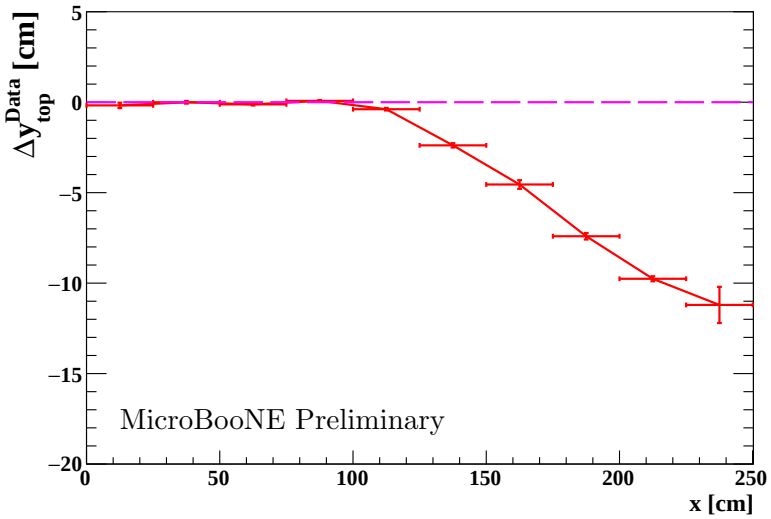

(b) $\Delta y^{\mathrm{Data}}_{\mathrm{top}}(x)$

Figure 7: Predicted/measured SCE distortions as a function of the drift coordinate at the top of the TPC for simulation, $\Delta y^{\mathrm{MC}}_{\mathrm{top}}(x)$ (a), and data, $\Delta y^{\mathrm{Data}}_{\mathrm{top}}(x)$ (b). The magenta dashed line represents the offsets expected if there were no SCE in the detector (zero). The offsets in data are found to be similar in magnitude as those predicted by simulation, though distortions near the TPC anode are found to be smaller than the simulation suggests.

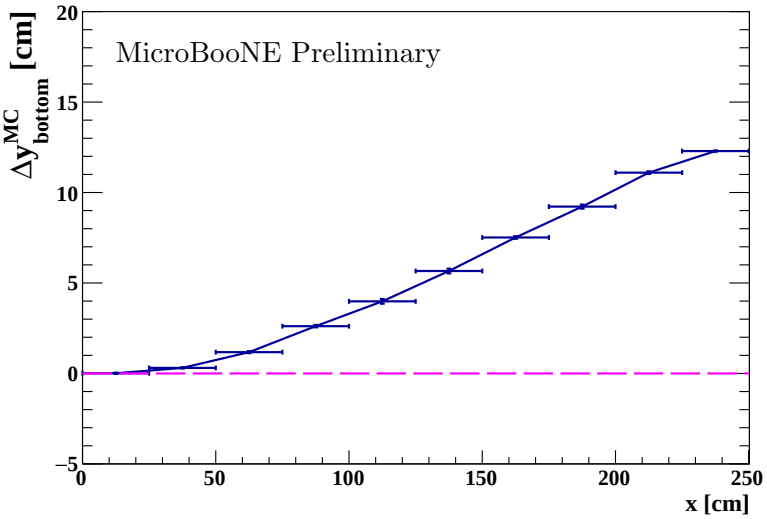

(a) $\Delta y^{\mathrm{MC}}_{\mathrm{bottom}}(x)$

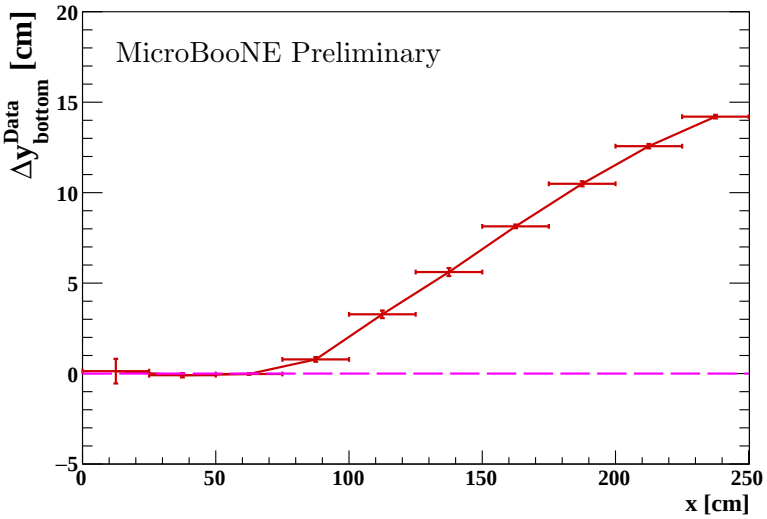

(b) $\Delta y^{\mathrm{Data}}_{\mathrm{bottom}}(x)$

Figure 8: Predicted/measured SCE distortions as a function of the drift coordinate at the **b**ottom of the TPC for simulation, $\Delta y^{\mathrm{MC}}_{\mathrm{bottom}}(x)$ (a), and data, $\Delta y^{\mathrm{Data}}_{\mathrm{bottom}}(x)$ (b). The magenta dashed line represents the offsets expected if there were no SCE in the detector (zero). The offsets in data are found to be similar in magnitude as those predicted by simulation, though distortions near the TPC anode are found to be smaller than the simulation suggests.

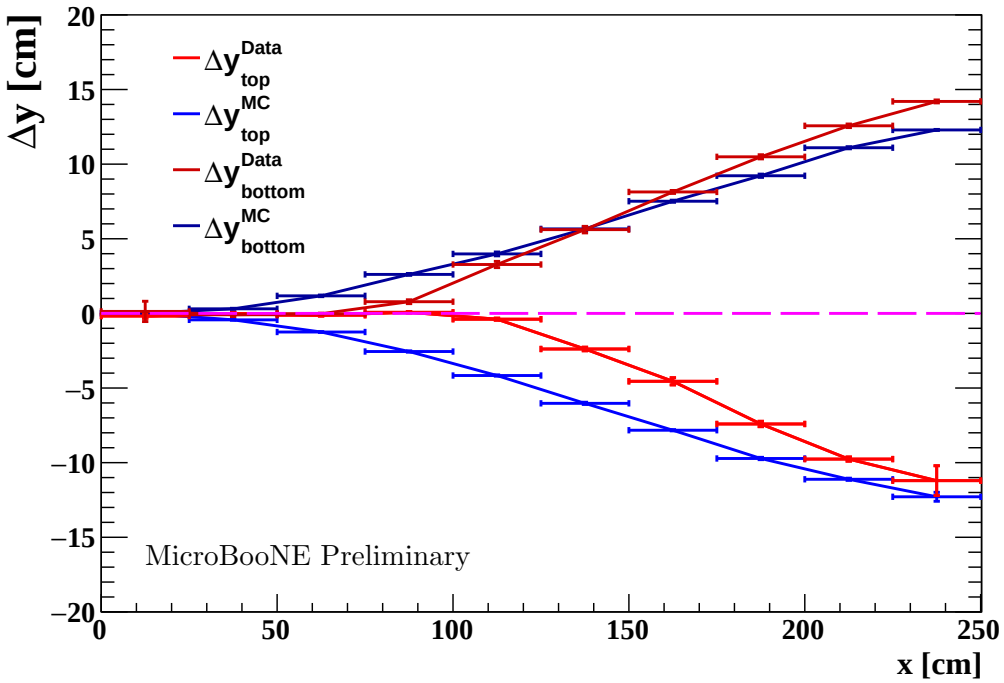

Figure 9: Predicted/measured SCE distortions as a function of the drift coordinate at both the top and bottom of the TPC, comparing data to MC. The magenta dashed line represents the offsets expected if there were no SCE in the detector.

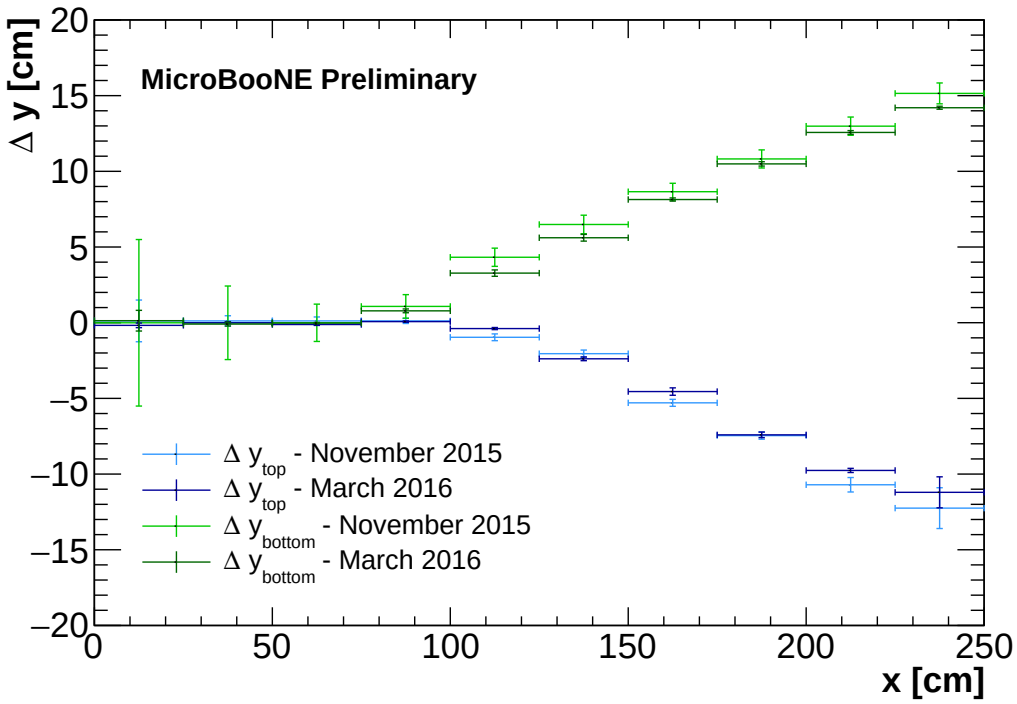

Figure 10: Measured SCE distortions as a function of the drift coordinate at both the top and bottom of the TPC, comparing data collected in November 2015 to data taken in March 2016. Very little change is seen between these two data-taking periods.

6.2 SCE Data/MC Comparison with Full Track Sample

In addition to a measurement of $\Delta y(x)$ described in Sec. 6.1, it is possible for us to measure $\Delta y(z)$ and $\Delta z(y)$ by utilizing a full sample of cosmic muon tracks in the TPC (without a tag from the MuCS). As for $\Delta y(x)$, these measurements can be made at the boundaries of the TPC where the distortions due to SCE are the largest. The $\Delta y(z)$ measurements are made at the TPC boundaries in y (top and bottom) while the $\Delta z(y)$ measurements are made at the TPC boundaries in z (upstream and downstream with respect to the direction of the beam). The advantage of using a full sample of cosmic muon tracks without tags from the MuCS is the capability to obtain full coverage of the TPC volume. The disadvantage is that information about the track location in the drift direction is lost, as currently information from the light-collection system is not being used. However, we show below that this information is not necessary for the measurement in question.

In order to measure $\Delta y(z)$ and $\Delta z(y)$ at the boundaries of the TPC, we again make use of the start/end points of reconstructed tracks. The distribution used is the position of track start/end points in y for $\Delta y(z)$ determination and in z for $\Delta z(y)$ determination. This distribution has a sharp "turn-on" feature near the TPC boundaries, which represents the maximal distortion at the cathode in terms of x coordinate, where the effect is largest, due to SCE in the direction orthogonal to the TPC boundary. By measuring the offset of this feature from the edge of the TPC, we can estimate the magnitude of the maximal spatial distortion due to SCE at the edges of the TPC in the y–z plane for both data and MC.

Results of measurements of $\Delta y_{\mathrm{top}}(z)$, $\Delta y_{\mathrm{bottom}}(z)$, $\Delta z_{\mathrm{upstream}}(y)$, and $\Delta z_{\mathrm{downstream}}(y)$ for both data and MC are shown in Fig. 11, Fig. 12, Fig. 13, and Fig. 14, respectively. It is important to note that the uncertainties on these measurements are obtained by eye for now, representing the difficulty in matching the features in the data and MC distributions; most often the "turn-on" feature is easily identified visually and determinable to within one histogram bin. Given that the uncertainties are determined by eye and represent an allowed range of variation, they should be interpreted as uniform posterior distributions. Some interesting features can be seen in Figs. 11-14. It appears that the SCE magnitude is lower than that predicted by the simulation near the top of the TPC, especially near the upstream side of the TPC in z. In general, the SCE offsets are found to be asymmetric in both y and z. This is yet more evidence that we may be seeing effects of liquid argon flow removing argon ions from the active TPC volume.

Another useful sample is a set of tracks that cross the cathode (where transverse SCE is largest in magnitude) at a known time determined via the use of a light-collection system. This sample would allow for the comparison of data and MC by measuring the offset of track start/end points from the TPC boundaries, looking for peaked features – a similar strategy to the one discussed in Sec. 6.1. In the future we expect to utilize such a sample for these measurements.

For now, the results strictly serve to illustrate the deviations of the SCE observed in data with respect to predictions from simulation throughout much of the active TPC volume near the boundaries, where distortions in the transverse directions are most

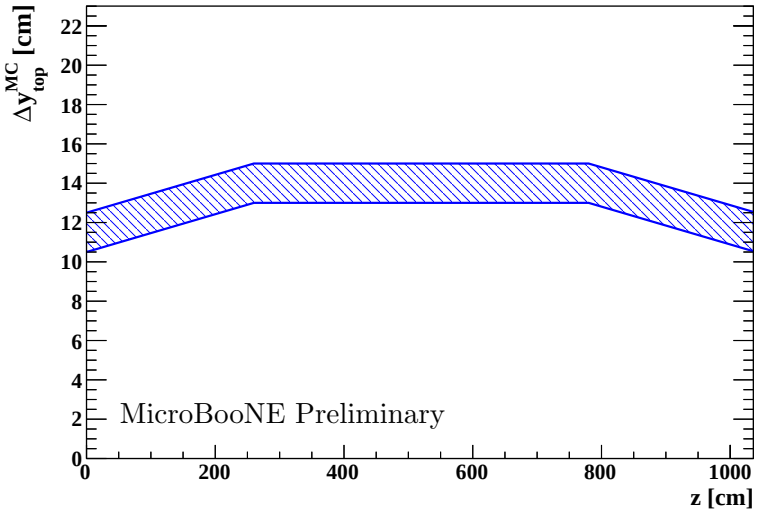

(a) $\Delta y^{\mathrm{MC}}_{\mathrm{top}}(z)$

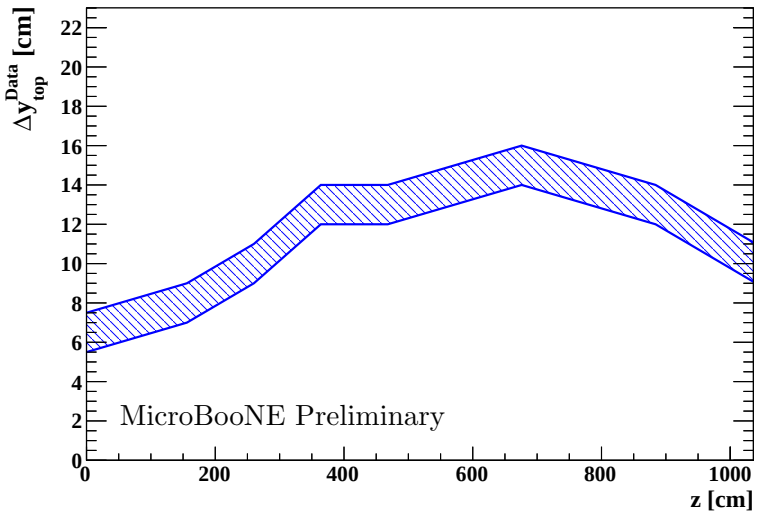

(b) $\Delta y^{\mathrm{Data}}_{\mathrm{top}}(z)$

Figure 11: SCE distortions as a function of z at the **t**op of the TPC for simulation, $\Delta y^{\mathrm{MC}}_{\mathrm{top}}(z)$ (a), and data, $\Delta y^{\mathrm{Data}}_{\mathrm{top}}(z)$ (b). The uncertainties are represented as bands and should be interpreted as uniform posterior distributions.

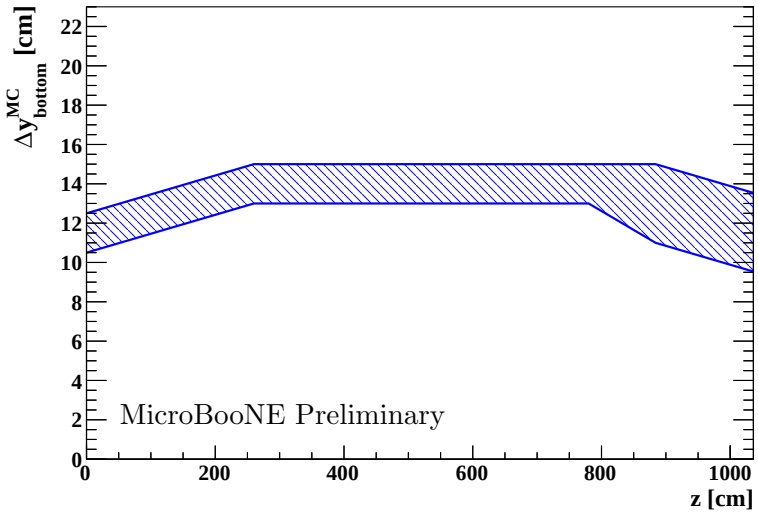

(a) $\Delta y^{\mathrm{MC}}_{\mathrm{bottom}}(z)$

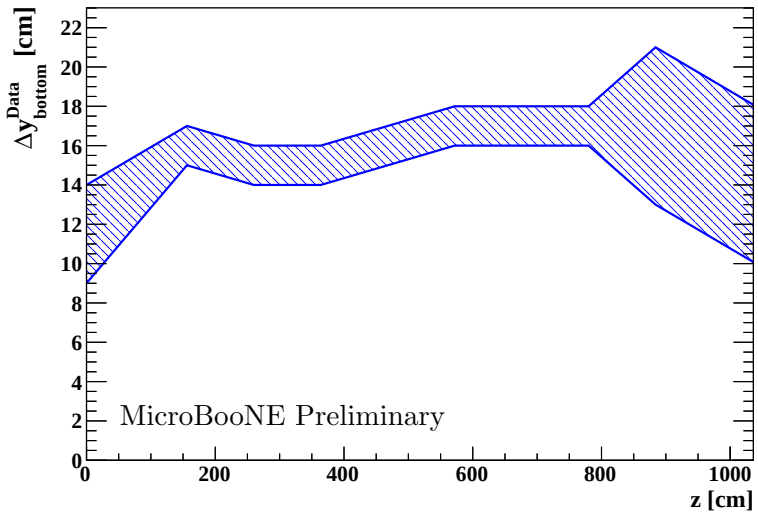

(b) $\Delta y^{\mathrm{Data}}_{\mathrm{bottom}}(z)$

Figure 12: SCE distortions as a function of z at the **b**ottom of the TPC for simulation, $\Delta y^{\mathrm{MC}}_{\mathrm{bottom}}(z)$ (a), and data, $\Delta y^{\mathrm{Data}}_{\mathrm{bottom}}(z)$ (b). The uncertainties are represented as bands and should be interpreted as uniform posterior distributions.

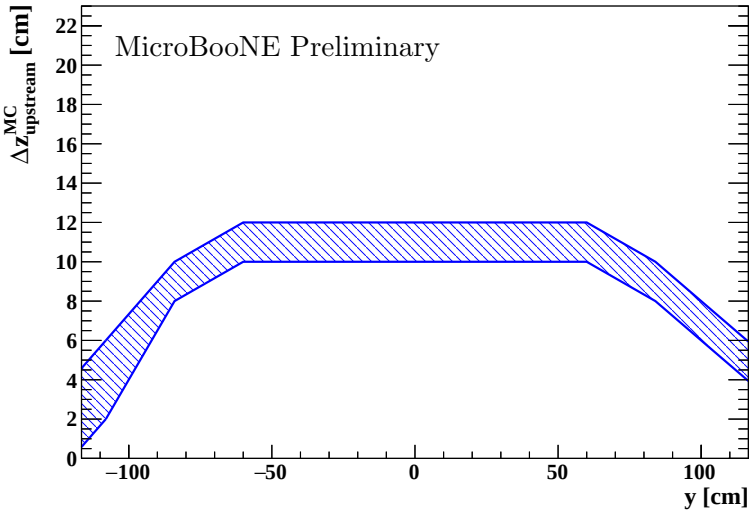

(a) $\Delta z^{\mathrm{MC}}_{\mathrm{upstream}}(y)$

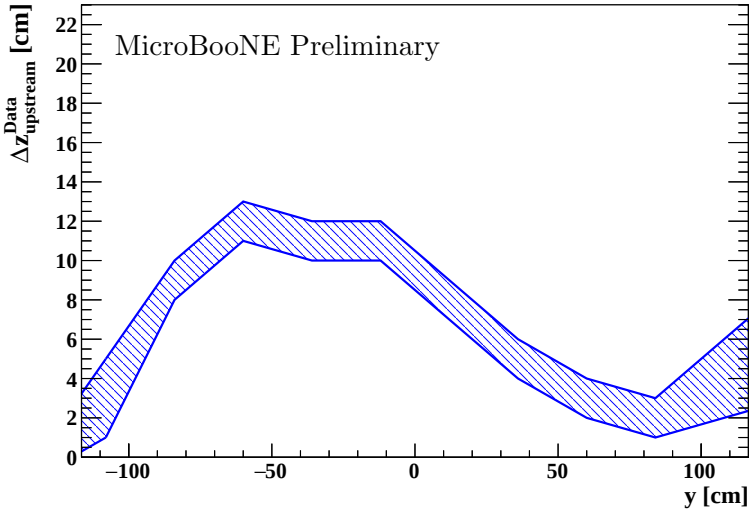

(b) $\Delta z^{\mathrm{Data}}_{\mathrm{upstream}}(y)$

Figure 13: SCE distortions as a function of y at the **u**pstream end of the TPC for simulation, $\Delta z^{\mathrm{MC}}_{\mathrm{upstream}}(y)$ (a), and data, $\Delta z^{\mathrm{Data}}_{\mathrm{upstream}}(y)$ (b). The uncertainties are represented as bands and should be interpreted as uniform posterior distributions.

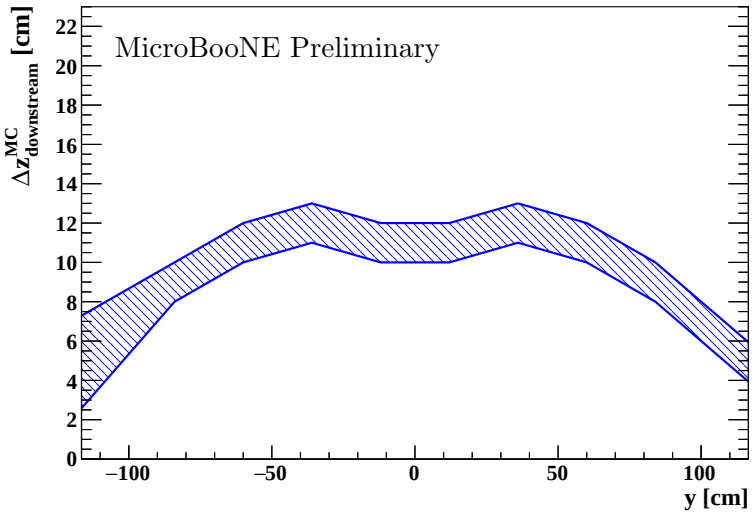

(a) $\Delta z^{\mathrm{MC}}_{\mathrm{downstream}}(y)$

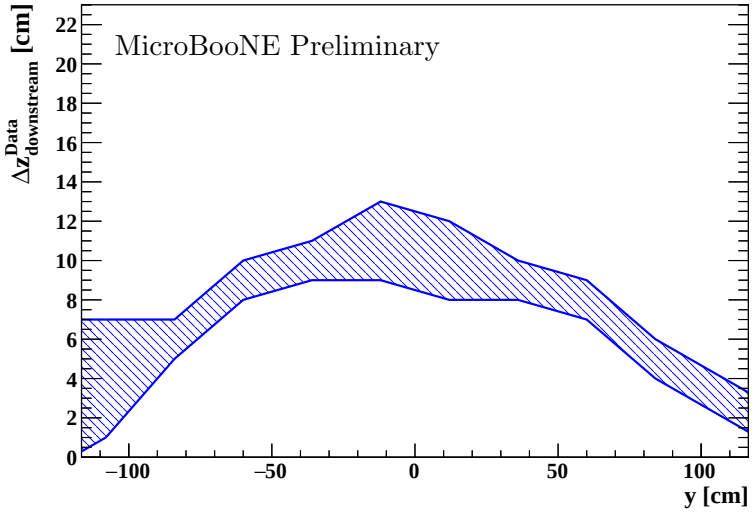

(b) $\Delta z^{\mathrm{Data}}_{\mathrm{downstream}}(y)$

Figure 14: SCE distortions as a function of y at the **d**ownstream end of the TPC for simulation, $\Delta z^{\mathrm{MC}}_{\mathrm{downstream}}(y)$ (a), and data, $\Delta z^{\mathrm{Data}}_{\mathrm{downstream}}(y)$ (b). The uncertainties are represented as bands and should be interpreted as uniform posterior distributions.

severe. They are not currently being utilized in a correction to track reconstruction. The use of these measurements in an improved data-driven space charge effect correction is the subject of a future analysis.

7 MuCS Data-Driven Correction

In addition to comparing data to MC for MuCS-triggered events, as was done in Sec. 6.1, the MuCS-merged TPC data was also used to derive and validate a correction to track start/end points. The additional information that comes from the MuCS-merger process allows the analysis to be extended to cut on photoelectrons information from the light collection system and use reconstructed MuCS angles and positions, along with their associated uncertainties from the strip widths, to compare with reconstructed tracks in the TPC.

This correction has been derived using the MuCS-merged dataset, as described in Sec. 4, which was collected at a different time than the MuCS-triggered dataset used in the previous section.

In particular, for this analysis, we require a MuCS-tagged track in each event with associated MuCS-merged information with between four and eight hit strips (inclusive) for each MuCS box (two for each layer of strips). In this way, we select only cosmic rays with a clear topology in the MuCS.We are also selecting only minimum-ionizing particles (MIPs) events, comparing the expected number of photoelectrons for a MIP with the number measured by the light collection system. It is also possible to explicitly remove all the events with an end point in the volume of the TPC, that should correspond to leftover stopping muon event, but the benefit to the analysis has been found to be negligible.

In this section we will quantify the SCE on the (x, y) plane for track start and end points. SCE-corrected data shows better agreement than non-SCE-corrected data with a Monte Carlo simulation that does not include SCE. In this case, our aim is to show that the SCE affects the angular distributions of the reconstructed tracks and that our correction, valid only for this sub-sample of events, is able to remove this distortion.

The MuCS data-driven SCE correction as a function of the (x,y) coordinates is based on four main assumptions, that follow from the Monte Carlo study of Sec. 3: (1) the effect is constant as a function of the z coordinate, (2) the effect is not constant in the y direction and the correction is zero at the vertical mid-plane of the TPC ($y = 0$), (3) in this region of the TPC only the y coordinate needs to be corrected and (4) the dependence of the SCE on the x and y coordinates for track start and end points can be factorized (an approximation).

In the region of the TPC covered by cosmic rays passing through both MuCS boxes, the SCE-corrected y coordinate y_{corr} will be given by:

$$y_{\text{corr}} = y_{\text{reco}} - \Delta y(x_{\text{reco}}, y_{\text{reco}}), \tag{7}$$

The difference $\Delta y(x_{\text{reco}}, y_{\text{true}})$ can be parametrized as:

$$\Delta y(x_{\text{reco}}, y_{\text{true}}) = \begin{cases} (f_{\text{top}}(x_{\text{reco}}) - y_{\text{top}})\, g(y_{\text{true}}), & \text{if } y_{\text{reco}} > 0 \\ (f_{\text{bottom}}(x_{\text{reco}}) - y_{\text{bottom}})\, g(y_{\text{true}}), & \text{if } y_{\text{reco}} < 0 \end{cases} \tag{8}$$

where:

- y_{top} and y_{bottom} are the y coordinates of the top and bottom border of the TPC, respectively;
- $f_{\text{top}}(x_{\text{reco}})$ ($f_{\text{bottom}}(x_{\text{reco}})$) is a quartic polynomial that gives the correction that must be applied as a function of the x coordinate for the top (bottom) part of the TPC;
- $g(y_{\text{true}})$, taken from simulation, is a scaling function that accounts for the y-dependence of Δy.

Having selected only MIP events, almost all the ends of the reconstructed tracks are located at the top or at the bottom-right border of the TPC (Fig. 17a). It is then not possible to measure the dependence of the SCE on the vertical axis (y) and the $g(y_{\text{true}})$ scaling function must be taken directly from simulation at the x position of the cathode x_{cathode}, that is:

$$\begin{aligned} g(y_{\text{true}}) &= \left| \frac{\Delta y^{MC}(x_{\text{cathode}}, y_{\text{true}})}{\Delta y^{MC}(x_{\text{cathode}}, y_{\text{top}})} \right| \approx \\ &\approx \left| \frac{\Delta y^{MC}(x_{\text{cathode}}, y_{\text{top}}/f(x_{\text{reco}}) \cdot y_{\text{reco}})}{\Delta y^{MC}(x_{\text{cathode}}, y_{\text{top}})} \right|, \end{aligned} \tag{9}$$

where we used the approximation: $y_{\text{true}} \approx y_{\text{top}}/f(x_{\text{reco}}) \cdot y_{\text{reco}}$ to make the scaling function $g(y_{\text{true}})$ depend on reconstructed information only. The Monte Carlo simulation of the scaling function $g(y_{\text{true}})$ (shown in Fig. 15) measured at the cathode coordinate x_{cathode} gives (parameters are expressed in cm):

$$g(y) = \left| -6.0 \times 10^{-3} y + 1.1 \times 10^{-7} y^2 - 1.9 \times 10^{-7} y^3 + 4.7 \times 10^{-4} \right|. \tag{10}$$

The correcting quantity $\Delta y(x_{\text{reco}}, y_{\text{true}})$ will be finally given by:

$$\Delta y(x_{\text{reco}}, y_{\text{true}}) = \begin{cases} (f_{\text{top}}(x_{\text{reco}}) - y_{\text{top}})\, g(x_{\text{cathode}}, y_{\text{top}}/f(x_{\text{reco}}) y_{\text{reco}}), \text{if } y_{\text{reco}} > 0 \\ (f_{\text{bottom}}(x_{\text{reco}}) - y_{\text{bottom}})\, g(x_{\text{cathode}}, y_{\text{top}}/f(x_{\text{reco}}) y_{\text{reco}}), \text{if } y_{\text{reco}} < 0. \end{cases} \tag{11}$$

In this way, even though we are introducing a dependence on the y_{reco} coordinates, it is possible to correct the end points at the cathode and the start/end points that are not exactly at the edge of the TPC.

The $g(x, y)$ function will be the same for top and bottom part of the TPC, because in the Monte Carlo they are assumed to be symmetrical (see Sec. 6.2). At the center

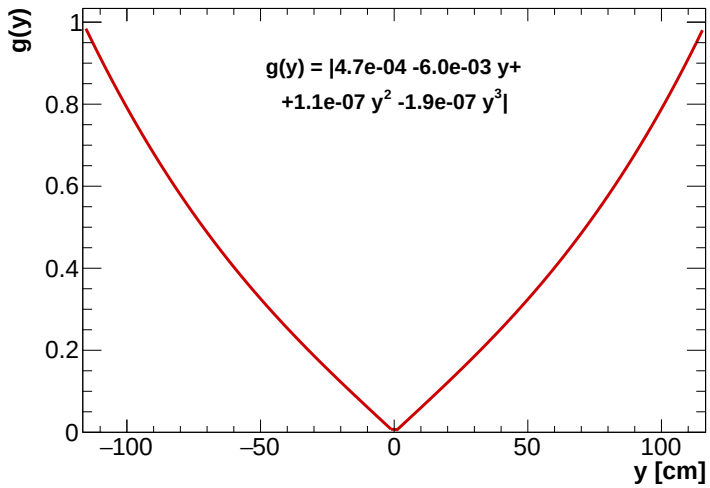

Figure 15: Monte Carlo simulation of the scaling function $g(y_{\text{true}})$ at x_{cathode}.

of the TPC ($y = 0$) the SCE effect on the y coordinate is zero, as expected from our assumptions.

In order to evaluate the $f_{\text{top}}(x_{\text{reco}})$ and $f_{\text{bottom}}(x_{\text{reco}})$ functions, the same procedure described in Sec. 6.1 has been followed. The two sets of points (one for the top part of the TPC and one for the bottom one) have been fitted by two quartic polynomials, which will correspond to $f_{\text{top}}(x)$ and $f_{\text{bottom}}(x)$, respectively (shown in Fig. 16). The fit gives (parameters are expressed in cm):

$$\begin{aligned} f_{\text{top}}(x) = &- 6.5 \times 10^{-2} x + 1.6 \times 10^{-3} x^2 - 1.3 \times 10^{-5} x^3 + \\ &+ 2.9 \times 10^{-8} x^4 + 1.2 \times 10^{2} \\ f_{\text{bottom}}(x) = &- 1.2 \times 10^{-1} x + 1.8 \times 10^{-3} x^2 - 5.3 \times 10^{-6} x^3 + \\ &+ 4.2 \times 10^{-9} x^4 - 1.1 \times 10^{2}. \end{aligned} \tag{12}$$

Finally, the SCE can be corrected by adjusting each y_{reco} coordinate of all track hits by $\Delta y(x_{\text{reco}}, y_{\text{reco}})$, as shown in Eq. (7). The contour lines of the function $y_{\text{reco}} - \Delta y(x_{\text{reco}}, y_{\text{reco}})$ are shown in Fig. 17b and the coordinates of the corrected start/end points of the tracks $(x_{\text{reco}}, y_{\text{corr}})$ are shown in Fig. 17c.

7.1 MuCS Residuals Distributions

The correction of the ends of the reconstructed tracks also affects the residuals distribution of the reconstructed angular coordinates, θ_{xy} and θ_{yz}, which represent the direction

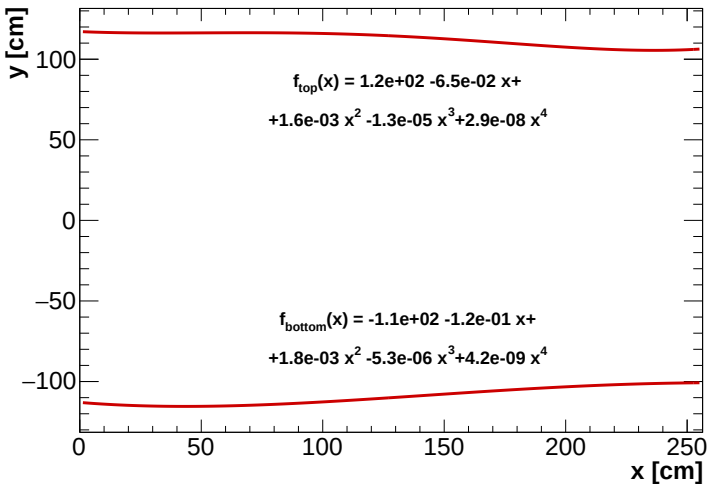

Figure 16: Plot of the $f_{\text{top}}(x)$ and $f_{\text{bottom}}(x)$ functions and respective fitted parameters.

of the track, measured using the start/end points. These coordinates are defined by:

$$\begin{aligned} \theta_{xy} &= \text{atan}\left(\frac{y_{\text{end}} - y_{\text{start}}}{x_{\text{end}} - x_{\text{start}}}\right) \\ \theta_{yz} &= \text{atan}\left(\frac{y_{\text{end}} - y_{\text{start}}}{z_{\text{end}} - z_{\text{start}}}\right), \end{aligned} \tag{13}$$

where $(x_{\text{start}}, y_{\text{start}}, z_{\text{start}})$ and $(x_{\text{end}}, y_{\text{end}}, z_{\text{end}})$ are the coordinates of the track start and end point, respectively.

We will show both the data angular distributions without SCE correction, calculated using the $(x_{\text{reco}}, y_{\text{reco}}, z_{\text{reco}})$ coordinates, and the SCE-corrected distribution, obtained by replacing the y_{reco} with the y_{corr} coordinate.

The Monte Carlo dataset has been generated without including the SCE in the simulation, to be compared with our SCE-corrected dataset.

For each MuCS-merged event we have simulated all the possible cosmic rays that can have the same geometrical hit pattern in the MuCS boxes. Then, we introduced the effects of the MuCS strip widths into the Monte Carlo distributions with a Gaussian smearing. The width of the Gaussian is different for each event and corresponds to the width of the distributions of the possible angles of the event hit pattern in the MuCS scintillator strips, computed by a Monte Carlo simulation.

The residual distributions are obtained by subtracting the θ_{xy} (θ_{yz}) value of the tagged tracks in MC or data from the θ_{xy} (θ_{yz}) value of the MuCS-merged track.

In particular, the SCE shifts the $\Delta\theta_{xy} = \theta_{xy}^{\text{MuCS}} - \theta_{xy}^{\text{tagged}}$ distribution towards negative values: when the y coordinates are moved towards the center of the TPC, the resulting θ_{xy} angle will be more inclined with respect to the vertical axis than expected (Fig. 18a).

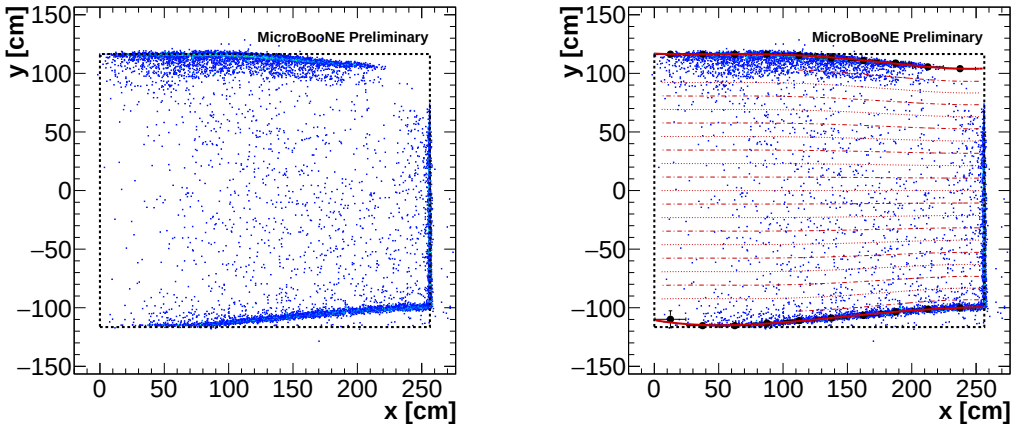

(a) Before SCE correction

(b) Fit of the data points

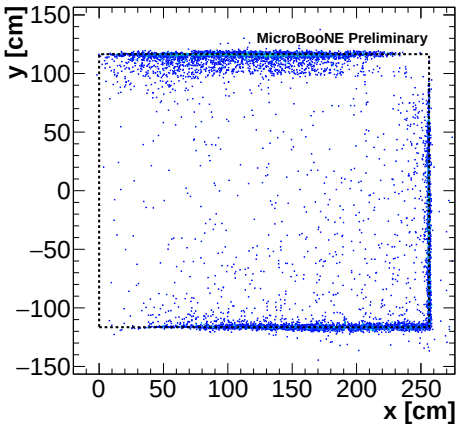

(c) After SCE correction

Figure 17: Ends of the reconstructed tracks (obtained with a Kalman filter algorithm) on the (x, y) plane for MuCS events before (a) and after (c) the SCE correction, along with the contour lines of the function $y_{\text{reco}} - \Delta y(x_{\text{reco}}, y_{\text{reco}})$ (b). The scatter in y of the points on the top of the TPC is due to reconstruction issues (e.g. dead wires splitting single tracks into multiple tracks).

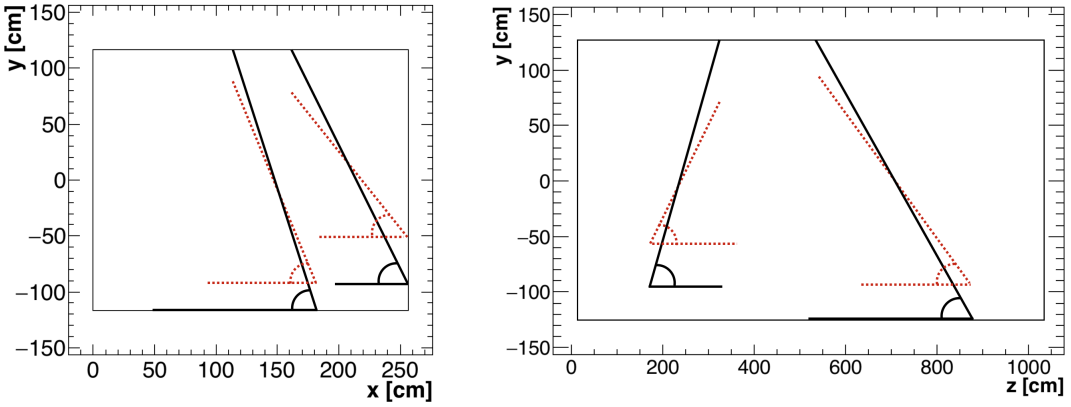

(a) XY plane

(b) ZY plane

Figure 18: Schematics of two reconstructed tracks that show the θ_{xy} and θ_{yz} angles before (dashed red line) and after (solid black line) the SCE correction. The SCE has been exaggerated to highlight the angular differences.

The mean of the uncorrected $\Delta\theta_{xy}$ distribution is $-2°$, while the mean of the SCE-corrected one is $-0.5°$. Thus, the correction of the effect shifts the residual distribution towards zero by $1.5°$ (Fig. 19a). The remaining bias is probably due to the SCE in the x direction, which was considered negligible, or to a small misalignment in the x-position of the top or bottom MuCS box.

The $\Delta\theta_{yz} = \theta_{yz}^{\text{MuCS}} - \theta_{yz}^{\text{tagged}}$ distribution, instead, is broadened by the SCE, because the y coordinates of the ends of the tracks are shifted towards the center of the TPC, while the z coordinates do not change, as shown in Fig. 18b. This effect, on average, gives smaller $\theta_{yz}^{\text{tagged}}$ values, resulting in a broader residual distribution. Correcting the SCE makes the distribution of this residual narrower, more in agreement with the MC simulation, shown in Fig. 19b. The angle distribution on the (y, z) plane is symmetric about $90°$ for MuCS tracks (see the MuCS configuration in Fig. 6), so we do not observe a shift of the peak that we have for the $\Delta\theta_{xy}$ distribution.

Residual differences between data and simulation can be due in part to multiple Coulomb scattering in the MuCS boxes, not included in the Monte Carlo (though multiple Coloumb scattering in the cryostat and insulation is included), or due to the broad range of cosmic muon energies above and below 4 GeV.

8 Conclusions and Future Work

The estimates of SCE distortions in the MicroBooNE TPC presented in this note offer a first glimpse at the differences of SCE in data with respect to predictions from simulation. By utilizing MuCS-tagged tracks and a more complete set of tracks (without t_0 corrections) we are able to extract deviations of spatial coordinates near the TPC boundaries where the distortions in the directions transverse to ionization drift are

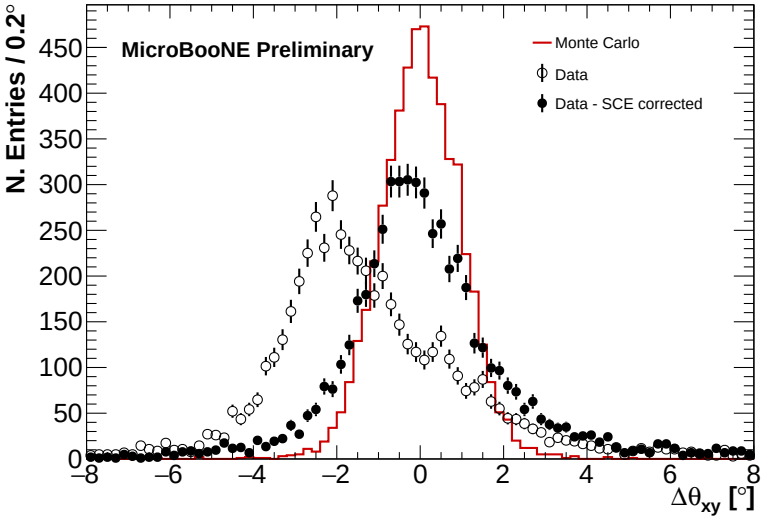

(a) $\Delta\theta_{xy}$ residual distribution

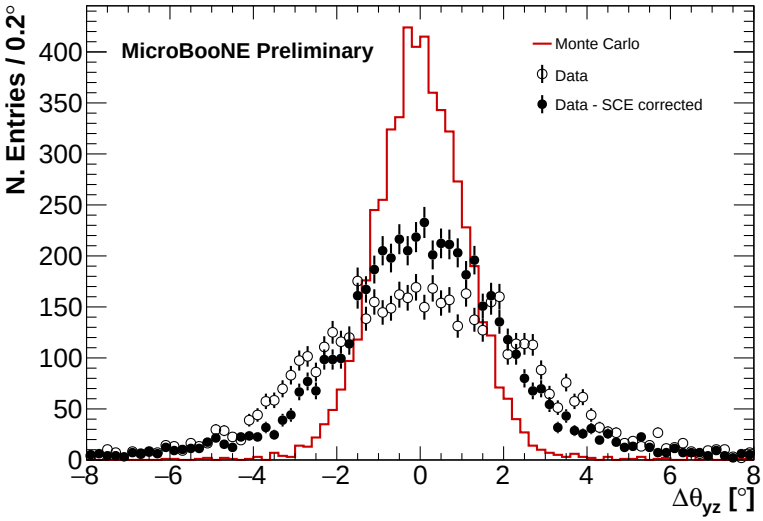

(b) $\Delta\theta_{yz}$ residual distribution

Figure 19: Residual distributions of θ_{xy} and θ_{yz} angular coordinates for data (blank points), SCE-corrected data (black points) and Monte Carlo (solid red lines). Monte Carlo tracks have been simulated without including the SCE.

largest. Compared to predictions from simulation, the SCE distortions measured in data are found to be very similar in both magnitude and shape, except for small deviations from the predicated value near the anode, where the effect is found to be non-existent. This observation is consistent with the flow of liquid argon removing ions from the active TPC volume.

The measurements of the distortions near the boundaries of the TPC in y allow us to apply a correction to MuCS data. This correction results in angular distributions of cosmic muon tracks in data that better match those of Monte Carlo track samples, removing bias and reducing smearing effects. After applying the correction, we are able to make a more precise alignment of the MuCS, though it is found that the original survey was quite accurate.

Much work remains in characterizing and calibrating out the SCE in the MicroBooNE TPC. By moving the MuCS, it is possible we can determine $\Delta z(x)$ at the TPC boundaries in z much like what we show for $\Delta y(x)$ at the TPC boundaries in y. Additionally, we have yet to establish a firm handle on SCE distortions present in the volume of the TPC, instead relying on the simulated SCE shape in the TPC volume for now. Ultimately, we will utilize the UV laser system to calibrate out the SCE in all three dimensions, obtaining $\Delta x(x, y, z)$, $\Delta y(x, y, z)$, and $\Delta z(x, y, z)$ in the TPC volume. Finally, while a look-back in data suggests that there are no significant time dependencies in the space charge configuration within the active TPC volume (on the timescale of several months – see Fig. 10), a more careful study looking at time-dependence of the SCE is planned.

References

[1] C. D. Child, *Discharge from Hot CaO*, Phys.Rev. 32, 492 (1911).

[2] I. Langmuir, *The Effect of Space Charge and Residual Gases on Thermionic Currents in High Vacuum*, Phys.Rev. 2, 450 (1913).

[3] M. Mooney, *The MicroBooNE Experiment and the Impact of Space Charge Effects*, `arXiv:1511.01563`.

[4] A. Ereditato et al., *A steerable UV laser system for the calibration of liquid argon time projection chambers*, JINST 9 (2014) T11007.

[5] K. McDonald, S. Palestini, *Space Charge in Ionization Detectors*, `http://physics.princeton.edu/~mcdonald/examples/spacecharge.pdf`.

[6] S. R. Soleti, *The Muon Counter System for the MicroBooNE experiment*, `arXiv:1604.07858 [physics.ins-det]`.

[7] E. D. Church, *LArSoft: A Software Package for Liquid Argon Time Projection Drift Chambers*, `arXiv:1311.6774 [physics.ins-det]`.

[8] C. Hagmann et al., *Cosmic-ray shower generator (CRY) for Monte Carlo transport codes*, Nuclear Science Symposium Conference Record, 2007. NSS '07. IEEE (Volume: 2).

[9] R. Fruhwirth, *Application of Kalman filtering to track and vertex fitting*, Nucl.Instrum.Meth. A262 (1987) 444-450.